## Title

Atlas of fetal metabolism during mid-to-late gestation and diabetic pregnancy.



## Journal

Cell, 187(1)

## Authors

Perez-Ramirez, Cesar
Nakano, Haruko
Law, Richard
et al.

## Publication Date

2024-01-04

## DOI

10.1016/j.cell.2023.11.011

Peer reviewed

HHS Public Access

Author manuscript

*Cell*. Author manuscript; available in PMC 2025 January 04.

Published in final edited form as:

*Cell*. 2024 January 04; 187(1): 204–215.e14. doi:10.1016/j.cell.2023.11.011.

*Correspondence: anakano@ucla.edu (A.N.), hchristofk@mednet.ucla.edu (H.R.C.).

AUTHOR CONTRIBUTIONS

HN, AN, and HRC conceptualized the examination of metabolic time course of developing organs. CAP, HN, AN, and HRC designed the study. CAP optimized and performed the in vivo [U-13C]glucose infusions, conducted all fetal tissue and plasma metabolite extractions, and performed the labeling analysis and targeted/untargeted metabolomics data analysis. HN set up timed pregnancies, collected blood and measured maternal glucose levels, counted fetal defects, and dissected fetal tissues. NM ran the LC-MS samples and performed raw file processing and targeted peak assignment. RCL and JOP analyzed the labeling data and developed models to assess nutrient sourcing and pathway utilization. JT assisted with fetal tissue processing and AP assisted with in vivo [U-13C]glucose infusions and metabolite extractions. CAP, HN, RCL, JOP, AN, and HRC conducted data interpretation and wrote and/or edited original manuscript with input from all authors.



DECLARATION OF INTERESTS

The authors declare no financial competing interests. HRC a member of the Cell Advisory Board.

INCLUSION AND DIVERSITY

We support inclusive, diverse, and equitable conduct of research. One or more of the authors of this paper self-identifies as an underrepresented ethnic minority in science. One or more of the authors of this paper self-identifies as a member of the LGBTQ+ community.

SUPPLEMENTAL TABLES

Table S1. Targeted metabolomics of fetal tissues and maternal plasma, related to Figure 1

Table S2. Metabolite isotopologue distribution from fetal tissues and maternal plasma, related to Figure 1

Table S3. Identified metabolites from targeted analysis that significantly differed between experimental groups, related to Figure 2.

Table S4. Untargeted metabolomics in placenta E18.5 and E10.5, related to Figure 6

SUPPLEMENTAL FIGURE LEGENDS

**Figure S1. Use of pregnant Akita mice to model maternal hyperglycemia, related to** Figure 1. (A) Table describing the number of heart and neural defects observed in fetuses from a representative cohort of wildtype (WT) versus Akita (AK) dams. Only fetuses lacking severe defects were used for this study. (B) Absolute plasma glucose levels (mM) in the pregnant wildtype dams relative to Akita dams used in this study after tracer infusion. Data are individual points and mean ± s.e.m. Statistical analyses were performed using multiple two-tailed *t*-tests with Holm-Sidak's multiple-comparisons adjustment. (C) Total $^{13}$C-enrichment (1-unlabeled) glucose in the plasma of the pregnant wildtype dams relative to Akita dams used in this study. Data are individual points and mean ± s.e.m. Statistical analyses were performed using multiple two-tailed *t*-tests with Holm-Sidak's multiple-comparisons adjustment. (D) Body weight before and after overnight fasting from a cohort of pregnant dams (E14.5-E15.5) n=7 for WT group and n=10 for AK group. Statistical analyses were performed using multiple two-tailed *t*-tests with Holm-Sidak's multiple-comparisons adjustment. (E) Maternal glucose and insulin levels throughout $^{13}$C-glucose tracer infusion in E15.5 euglycemic (WT) versus hyperglycemic (AK) dams (n=3 for each) Data are mean ± s.e.m. Statistical analyses were performed using two-tailed *t*-tests. (F-G) Time development of the weighted glucose enrichment in maternal plasma (F) and fetal tissues (G). For maternal plasma (F), linear regression analysis is represented by the dotted line with the slope values for both WT and AK maternal plasma (n=3–4 per timepoint for both WT and AK). For both maternal plasma (F) and fetal tissues (G), enrichment curves were determined by fitting an exponential rise to maximum (one-phase association) model. For fetal tissues from WT dams n=4 per timepoint and from AK dams n=1–2 per timepoint

**Figure S2. Significant features of metabolic profiles in maternal plasma and fetal tissues between wildtype and Akita dams, related to** Figure 2. (A) Venn diagram representation of the number of metabolites that significantly differed between experimental groups. Statistical significance was determined via Two-way ANOVA with FDR (Benjamini-Hochberg) controlling procedure.

**Figure S3. GABA measurements in fetal tissues, related to** Figure 3. (A) GABA levels from E12.5 fetal brains dissected from dams without fasting, anesthesia or glucose tracing. Data is represented relative to WT samples. Data are individual points and mean ± s.e.m. Statistical analyses were performed using multiple two-tailed *t*-tests with adjustment using the Benjamini-Hochberg FDR controlling method. n=6 for WT group and n=4 for AK group (B) M+2 GABA labeling normalized to M+2 glutamate levels compared between E12.5 fetal brains from WT and AK dams. Data is represented relative to WT samples. Tukey method was applied for plotting whiskers and outliers. Statistical analyses were performed using multiple two-tailed *t*-tests with Holm-Sidak's multiple-comparisons adjustment.

**Figure S4. Isotope tracing in fetal tissue elucidates metabolic strategy, related to** Figure 4. (A) Labeling of fetal asparagine normalized to maternal asparagine labeling in wildtype (WT) and Akita (AK) dams. (B) Labeling of intracellular glutamate (vertical) compared to intracellular α-ketoglutarate (horizontal). The dashed line represents the line of parity, where glutamate and α-ketoglutarate labeling are equal. (C) Fraction of fully labeled intermediates in the pentose phosphate pathway. (D) Fraction of M+2 (2 carbons labeled) intermediates in the TCA cycle. Catabolism of labeled glucose to the TCA cycle via pyruvate dehydrogenase forms doubly rather than fully labeled citrate. (E) Schematic of glycogen breakdown relative to glycolysis. Glycogen, which has slow turnover relative to glucose, introduces unlabeled hexose phosphates into glycolysis. G6P, glucose-6-phosphate; G1P, glucose-1-phosphate. (F) Fraction of fully labeled glycolytic intermediates (glucose, glucose-6-phosphate, phosphoglycerate, pyruvate, lactate) in fetal hearts and brains from WT and AK dams compared to maternal glucose and lactate labeling. Green bands represent

# ATLAS OF FETAL METABOLISM DURING MID-TO-LATE GESTATION AND DIABETIC PREGNANCY

**Cesar A Perez-Ramirez**[1,4,7], **Haruko Nakano**[2,7], **Richard C Law**[3], **Nedas Matulionis**[1], **Jennifer Thompson**[2], **Andrew Pfeiffer**[1], **Junyoung O Park**[3,5,6,8], **Atsushi Nakano**[2,4,5,6,8,*], **Heather R Christofk**[1,4,5,6,8,9,*]

[1]Department of Biological Chemistry, David Geffen School of Medicine, University of California, Los Angeles (UCLA), Los Angeles, CA 90095, USA.

[2]Department of Molecular, Cell, and Developmental Biology, UCLA, Los Angeles, CA 90095, USA.

[3]Department of Chemical and Biomolecular Engineering, UCLA, Los Angeles, CA 90095, USA.

[4]Eli and Edythe Broad Center of Regenerative Medicine and Stem Cell Research, UCLA, Los Angeles, CA 90095, USA.

[5]Jonsson Comprehensive Cancer Center, UCLA, Los Angeles, CA 90095, USA.

[6]Molecular Biology Institute, UCLA, Los Angeles, CA 90095, USA.

[7]These authors contributed equally

[8]Senior author

---

maternal plasma labeling of glucose, and purple bands represent maternal labeling of lactate. Means ± s.e.m. are represented by a dashed line and the width of the bands. (G) Comparison of lactate labeling contribution to G6P in WT and AK tissues. Negative values indicate substantial glycogenolysis. Statistical analyses were performed using multiple two-tailed *t*-tests with Holm-Sidak's multiple-comparisons adjustment.

**Figure S5. Progressive decrease in [U-$^{13}$C]glucose enrichment in fetal tissue nucleotides, related to** Figure 5. (A) Blue to red scale: Heatmap representing the log2 fold changes in nucleotide pool levels relative to E10.5 fetal tissues (placenta, heart, and brain) or E12.5 for fetal livers from Akita dams. White to red scale: Heatmap representing the total $^{13}$C-enrichment (1-unlabeled) of nucleotides in fetal tissues from Akita dams during mid-to-late gestation. (B-D) Relative IMP (B), GMP (C), and CMP (D) pool levels across fetal tissues. For fetal tissues from WT dams, data is represented relative to the mean of WT E10.5 samples. For fetal tissues from Akita (AK) dams, data is represented relative to the mean of AK E10.5 samples. (E-G) Normalized total $^{13}$C-enrichment (1-unlabeled) of IMP (E), GMP (F), and CMP (G) across fetal tissues. For each fetal tissue, the nucleotide labeled pool (1-unlabeled) was normalized to its respective total $^{13}$C-enrichment (1-unlabeled) of glucose from maternal plasma. Data are individual points and mean ± s.e.m. Statistical analyses were performed using multiple two-tailed *t*-tests with Holm-Sidak's multiple-comparisons adjustment.

**Figure S6. Untargeted analysis reveals increased levels of histidine derived metabolites in late gestation, related to** Figure 6. (A) MetaboAnalyst functional analysis of negative ion mode untargeted data of E18.5 placentas from wildtype dams relative to E10.5 (left graph). MetaboAnalyst functional analysis of positive ion mode (middle graph) and negative ion mode (right graph) untargeted data of E18.5 placentas from Akita dams relative to E10.5 with representation of raw p-values. Top 5 pathway terms are listed (B) Extracted ion chromatographs of imidazole-4-acetate, urocanate and histamine from representative fetal tissue samples compared to pure chemical standard. RT denotes retention time. Representative fetal tissue samples shown were from a E18.5 fetus (#1) of a wildtype dam (Mouse A). (C) Relative pool levels of histidine derived metabolites in maternal plasma. For maternal plasma from WT dams, data is represented relative to the mean of WT E10.5 samples. For maternal plasma from Akita (AK) dams, data is represented relative to the mean of AK E10.5 samples. Data are individual points and mean ± s.e.m. Statistical analyses were performed using multiple two-tailed *t*-tests with adjustment using the Benjamini-Hochberg FDR controlling method. (D) Relative pool levels of histidine and its derived metabolites, urocanate, histamine, and imidazole-4-acetate across E12.5 and E18.5 fetal tissues from wildtype (WT) and Akita (AK) dams without fasting, tracer infusion, and anesthesia. For fetal tissues from WT dams, data is represented relative to the average of WT E12.5 samples. For fetal tissues from Akita (AK) dams, data is represented relative to the mean of AK E12.5 samples. Relative pool levels of histamine and imidazole-4-acetate are shown using a log2 scale for the y-axis. Statistical analyses were performed using multiple two-tailed *t*-tests with adjustment using the Benjamini-Hochberg FDR controlling method. Fetal tissues dissected from non-fasted mice n=17–18 (10–11 for WT group and 7 for AK group).

[9]Lead contact

## SUMMARY

Mounting evidence suggests metabolism instructs stem cell fate decisions. However, how fetal metabolism changes during development and how altered maternal metabolism shapes fetal metabolism remain unexplored. We present a descriptive atlas of *in vivo* fetal murine metabolism during mid-to-late gestation in normal and diabetic pregnancy. Using $^{13}$C-glucose and LC-MS, we profiled the metabolism of fetal brains, hearts, livers, and placentas harvested from pregnant dams between embryonic days (E)10.5 and 18.5. Our analysis revealed metabolic features specific to a hyperglycemic environment and signatures that may denote developmental transitions during euglycemic development. We observed sorbitol accumulation in fetal tissues and altered neurotransmitter levels in fetal brains isolated from hyperglycemic dams. Tracing $^{13}$C-glucose revealed disparate fetal nutrient sourcing depending on maternal glycemic states. Regardless of glycemic state, histidine-derived metabolites accumulated in late-stage fetal tissues. Our rich dataset presents a comprehensive overview of *in vivo* fetal tissue metabolism and alterations due to maternal hyperglycemia.

## Graphical Abstract

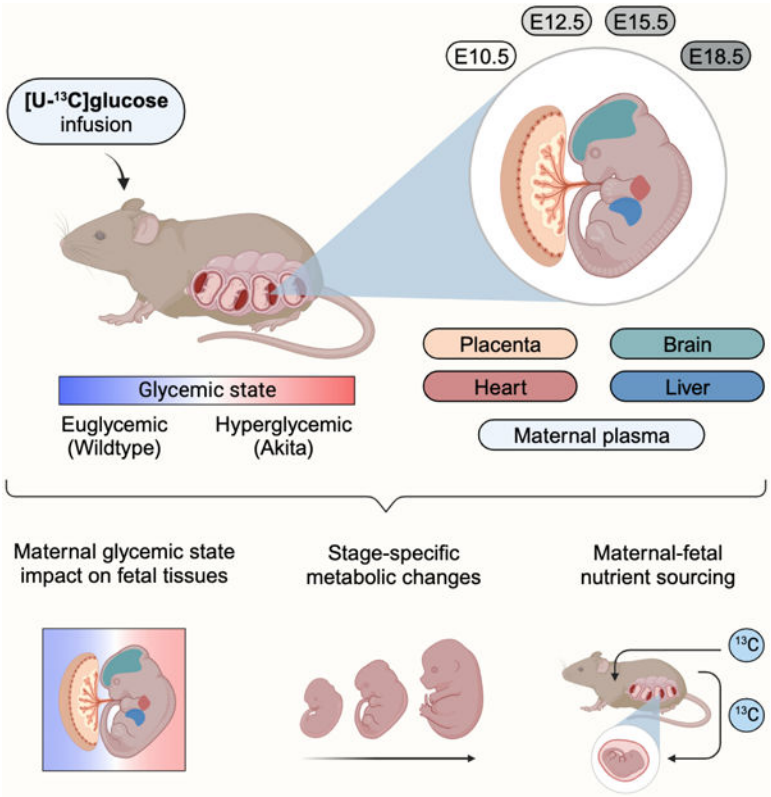


## IN BRIEF:

A descriptive atlas of murine metabolism in utero during mid-to-late gestation in normal and diabetic pregnancy reveals the impact of maternal hyperglycemia on fetal tissues. $^{13}$C-glucose tracing highlights differences in fetal tissue nutrient sourcing in diabetic pregnancies.

## INTRODUCTION

Maternal nutrition and fetal development are inseparable. Dietary interventions during pregnancy promote maternal health and reduce the incidence of fetal developmental defects. For instance, iron supplementation prevents intrauterine growth restriction during pregnancy, and folic acid supplementation reduces the incidence of fetal neural tube defects. [1,2] However, not much is known about how fetal metabolism is shaped during development, nor how prevalent clinical conditions affecting maternal metabolism impact developing fetuses. Recent studies have begun to characterize metabolic plasticity in the mouse pre-implantation embryo [3] and compartmentalization during embryonic day (E)9.5–13.5. [4] But fetal metabolism during mid-to-late gestation, when the fetus nears completion of its independent circulatory system, remains unexplored.

Maternal diabetes is a growing clinical problem in the US and worldwide: the rate of diabetes cases amongst pregnant individuals per 1,000 live births in the US rose from 47.6 in 2011 to 63.5 in 2019. [5] This adverse trend is due to an increased incidence of gestational diabetes and type 2 diabetes in younger patients prior to pregnancy. Maternal hyperglycemia is associated with a four-fold increased risk of congenital heart defects and increased risk of neurodevelopmental defects. [6,7,8] Previously, we found that high glucose levels impair cardiac maturation *in vitro* through excessive nucleotide metabolism. [9] However, the *in vivo* impact of maternal hyperglycemia on the metabolism of the developing fetus remains unknown and may shed light mechanistically on the cause of congenital defects in diabetic pregnancy.

Remarkable studies in mice have provided an increasingly detailed view of mammalian development from the perspective of genomics and transcriptomics. [10,11,12] Here we provide an additional layer to the understanding of mammalian development by quantifying the metabolic landscape of the developing fetus at a multi-tissue level and examining how maternal hyperglycemia shapes this landscape. Using LC-MS and [U-$^{13}$C]glucose tracing, we measured the metabolic profile of fetal tissues (placenta, heart, liver, brain) dissected from pregnant mice during mid-to-late gestation. We present an expansive metabolomic atlas of fetal tissues that offers insights into metabolite level dynamics and pathway utilization under euglycemia and hyperglycemia. Our rich dataset reveals metabolic signatures that reflect the impact high glucose exposure *in utero* has on fetal tissue metabolism and can be leveraged toward the design of improved strategies to meet the nutritional needs of the fetus.

## RESULTS

### Fetal metabolomics in euglycemia and hyperglycemia

To model diabetic pregnancy, we used the hyperglycemic Akita mouse, which produces mildly defective but surviving offspring through the mid- and late-gestation periods. These mice harbor a heterozygous mutation in the Ins2 gene, leading to the development of adult-onset diabetes. [13] In the C57BL/6 background, Akita dams were crossed with wildtype males to create a diabetic pregnancy condition in which fetuses are exposed to a hyperglycemic environment. [9] Offspring of Akita dams showed some heart and neural tube

defects; however, most defects were mild with the majority being suitable for LC-MS-based metabolomic analysis (Figure 1A and S1A).

We set out to map the metabolomic profile of fetal tissues collected from pregnant Akita dams versus wildtype dams throughout development, specifically during mid-to-late gestation. To accomplish this goal, timed mouse pregnancies were set to stages E10.5, E12.5, E15.5, and E18.5. Both wildtype and diabetic (Akita) dams were fasted overnight and infused with [U-$^{13}$C]glucose prior to fetal tissue collection to trace $^{13}$C through metabolic pathways. Following three hours of tracer infusion, metabolites were extracted from dissected fetal placenta, brain, heart, and liver (Figure 1B). Maternal plasma samples were collected for glucose measurements and LC-MS metabolite analysis to ensure elevated glucose levels in the Akita dams and similar $^{13}$C-glucose enrichment in wildtype and Akita dams (Figure S1B and S1C). On a cohort of E15.5 pregnant mice, we confirmed that no significant changes in mouse weights were observed due to overnight fasting in wildtype or Akita dams (Figure S1D). Furthermore, maternal plasma sampling and serial cesarean sections were performed throughout a four-hour infusion of [U-$^{13}$C]glucose, enabling assessment of glucose, insulin, and labeling dynamics. Insulin levels were comparable between wildtype and Akita dams at each time point of the tracer infusion, while blood glucose levels showed a larger response in Akita dams relative to wildtype dams at three hours of infusion (Figure S1E). The time development of $^{13}$C-glucose enrichment in maternal plasma and fetal tissues corroborated that (pseudo-)steady state had been achieved in circulation and fetal tissues from both wildtype and Akita dams at three hours post tracer infusion (Figure S1F–G).

This experimental setup yielded a high-quality dataset providing three analytical dimensions within the context of development: 1) developmental stage, 2) fetal tissue origin, and 3) maternal glycemic state. Our data analysis pipeline involved both targeted and untargeted metabolomics as well as isotope tracing from [U-$^{13}$C]glucose to provide insights into pathway utilization and nutrient sourcing (Figure 1C). Targeted analysis of metabolomics data involved the cross-referencing to a metabolite library composed of 162 metabolites (Table S1). Across all tissues, gestational stages, and maternal glycemic state, we generated a comprehensive quantification of metabolite levels for further analysis (Figure 1D). Furthermore, we measured the isotopologues of each metabolite to gain further insights into metabolic fluxes (Table S2). Fractional $^{13}$C enrichment analysis showed disparate activities across developmental stages and metabolic pathways (Figure 1E). In all fetal tissues, glycolytic metabolites were mostly labeled between E10.5 and E15.5, but glycolytic metabolite labeling sharply decreased in E18.5 fetal tissues. Glycolytic metabolites in the liver and the brain of E18.5 fetuses from wildtype dams were significantly less labeled than those from Akita dams, indicating a growing disparity in the sourcing of these intermediates depending on maternal glycemic state. The pentose phosphate pathway (PPP) $^{13}$C enrichment suggested peak activities at different development stages for different tissues: the PPP activity in the placenta and the liver peaked at E10.5 while in the heart and the brain it peaked at E12.5 and E15.5. Multiple nutrients contribute to the TCA cycle metabolite pool. Thus, its $^{13}$C enrichment indicated the direct and indirect contribution of glucose to the TCA cycle. The fetal tissues from wildtype dams were significantly more labeled in the early E10.5 and E12.5 stages but the labeling in fetal tissues from Akita dams

overtook the wildtype counterparts by E18.5, indicative of sustained glucose catabolism in hyperglycemic development.

## Maternal hyperglycemia causes sorbitol accumulation in fetal tissues

We performed two-way ANOVA with an FDR controlling procedure to highlight the substantial number of differences in our targeted metabolomics datasets (Figure S2A and Table S3). Looking closely at glucose metabolism, this dataset revealed markedly increased sorbitol levels in fetal tissues harvested from Akita versus wildtype dams (Figure 2A). Sorbitol is generated from glucose through the action of aldose reductase as part of the polyol pathway (Figure 2B). To assess the extent of sorbitol accumulation in fetal tissues harvested from Akita versus wildtype dams, we determined the increase in sorbitol levels relative to E10.5 fetal tissues from wildtype dams. We observed increased sorbitol levels in fetal placentas, hearts, livers, and brains exposed to maternal hyperglycemia. Fetal brains isolated from Akita dams during E15.5 and E18.5, in particular, showed the largest sorbitol accumulation relative to E10.5 fetal brains isolated from wildtype dams (Figure 2C). Sorbitol accumulation in adult diabetic patients can lead to tissue osmotic stress and contributes to the damage that occurs in insulin-independent tissues such as retina, kidney, and nerves. [14] Our data revealed that fetuses exposed to maternal hyperglycemia are not protected from sorbitol accumulation and suggested that sorbitol accumulation during fetal development may contribute to the higher incidence of developmental defects observed during diabetic pregnancy.

## Maternal hyperglycemia alters amino acid metabolism in the fetal brain

We were curious about how maternal hyperglycemia altered broader fetal metabolism. We observed changes in amino acid levels in fetal tissues harvested from wildtype versus Akita dams (Figure 3A). Over the developmental stages, most amino acid levels in fetal hearts harvested from Akita dams decreased to a lesser extent compared to fetal hearts harvested from wildtype dams, while those in Akita fetal livers and brains trended up more strongly. Most notably, fetal brain aspartate levels presented different trends over the developmental timeframe assessed in fetuses harvested from wildtype versus Akita dams (Figure 3B). In fetal brains isolated from wildtype dams, aspartate levels increased roughly 2-fold from E10.5 to E12.5, however in fetal brains isolated from Akita dams, aspartate levels remained unchanged from E10.5 to E12.5 and instead increased roughly 2-fold between E12.5 to E15.5 (Figure 3B). These changes are in contrast to fetal brain asparagine levels which remained unchanged across the developmental timeframe and conditions assessed (Figure 3B). The levels of glutamate and glutamate-derived gamma-aminobutyric acid (GABA) were also different in fetal brains harvested from wildtype versus Akita dams (Figure 3C). Glutamate and GABA levels were lower in E10.5 and E12.5 fetal brains isolated from Akita dams relative to E10.5 and E12.5 fetal brains isolated from wildtype dams. Consistently, GABA levels were also lower in E12.5 fetal brains isolated from Akita dams without anesthesia or overnight fasting (Figure S3A). Tracing $^{13}C$ through GABA synthesis, we observed similar M+2 GABA labeling normalized to M+2 glutamate in E12.5 fetal brains from wildtype and Akita dams (Figure S3B). Lower levels of these neurotransmitters may contribute to the higher incidence of congenital brain defects observed in fetuses exposed to maternal hyperglycemia. [15]

## Isotope tracing reveals fetal growth strategies

Tracing [U-$^{13}$C]glucose through central carbon metabolism revealed how fetal tissues source biomass building blocks. Using the principle that a metabolite's $^{13}$C labeling fraction cannot be greater than that of its stable $^{13}$C source, we traced $^{13}$C at two different levels: 1) the whole-body level, which reveals nutrient exchange fluxes, and 2) the tissue level, which reveals fluxes through metabolic pathways. At the whole-body level, we considered the fetal circulatory system to be connected to maternal circulation through a path from the placenta to the liver, to the heart, and to the brain (Figure 4A). [16,17] We observed that seven non-essential amino acids (Asp, Asn, Glu, Gln, Pro, Ser, and Gly) were $^{13}$C-labeled in fetuses, and of those seven, aspartate and glycine were not labeled in maternal plasma (Figure 4B). Therefore, aspartate and glycine were entirely synthesized by fetal tissues. Maternal and fetal metabolism contributed to five amino acids (Asn, Glu, Gln, Pro, and Ser) in fetuses, and the 13 other amino acids were entirely sourced from the dam. The uptrend of glutamate labeling through the circulatory path in E15.5 and E18.5 fetuses implied that every fetal tissue made its own glutamate, whereas the serine labeling peaking in the liver implied that the heart and the brain may not necessarily make their own serine and depend on serine overflow from the liver. Similarly, proline in the placenta may be contributing to fetal tissues in E10.5 before the liver and the brain develops the proline synthesis capability as evidenced in E15.5 fetuses. The time development of asparagine labeling revealed that asparagine biosynthesis in fetal livers isolated from wildtype dams begins at E18.5 while it begins earlier at E15.5 in fetal livers isolated from Akita dams (Figure S4A).

At the tissue level, $^{13}$C tracing revealed the metabolic pathways responsible for the labeling of amino acids (Figure 4C). Tissue metabolites can gain $^{13}$C via maternofetal [U-$^{13}$C]glucose transport through the placenta and via transport of other circulating metabolites the dam had produced from [U-$^{13}$C]glucose. [18,19] Fetal aspartate was similarly or less labeled than malate, a proxy for oxaloacetate that is the direct precursor of aspartate, but more labeled than plasma aspartate (Figure 4D). Fetal glutamate labeling was consistently higher than both plasma glutamate labeling and fetal glutamine labeling but comparable to tissue α-ketoglutarate labeling (Figure 4E and S4B). Given that the labeling source (i.e. glucose) is at steady state and that a product pool cannot be more labeled than its precursor pool, these observations implied that fetal tissues *de novo* synthesized aspartate and glutamate via anaplerosis and the TCA cycle.

We set out to determine if the $^{13}$C labeling in fetal tissue glycolytic intermediates was sourced directly or indirectly from glucose. In other central carbon metabolic pathways, progressive labeling of individual metabolite pools indicated unambiguously how $^{13}$C moved across each pathway (Figure S4C and S4D). However, the labeling of glycolytic metabolites displayed more nonmonotonic profiles. Since circulating lactate is another high-flux carbon source, we considered three scenarios that yield different $^{13}$C labeling: the major carbon source(s) being 1) plasma glucose, 2) both plasma glucose and lactate, and 3) plasma lactate (Figure 4F and S4E). [20] Additionally, we considered the potential introduction of unlabeled hexose phosphate via glycogenolysis. [21] In the placenta, glycolytic labeling reflected the contribution of both plasma glucose and plasma lactate, which had been labeled in the dam across mid-to-late gestation (Figure 4G and S4F). The liver, on the

other hand, displayed disparate glycolytic labeling signatures between fetuses from wildtype and Akita dams. In E10.5 and E12.5, fetal liver from wildtype dams displayed ascending labeling gradient across glycolysis, indicating gluconeogenesis from $^{13}$C-labeled lactate and perhaps dilution of hexose $^{13}$C labeling by glycogenolysis (Figure 4G and S4G). However, $^{13}$C glucose labeling was higher in fetal livers harvested from Akita dams across mid-to-late gestation and more similar to the level of glucose labeling in maternal circulation. Taken together, maternal hyperglycemia not only alters the source of carbon backbones in fetuses but also sustains glucose contribution to amino acid biosynthesis in late gestation.

## Fetal nucleotide synthesis slows in mid-to-late gestation

Nucleotides are in high demand during rapid cell division, yet they are not available via circulation. Thus, we investigated how fetal tissues manage nucleotide biosynthesis. We observed fetal tissue-specific increases in nucleotides in the heart, liver, and brain - but not placenta - at E12.5, E15.5, and E18.5 relative to E10.5 (Figure 5A and S5A). Nucleoside monophosphates and diphosphates, but not nucleoside triphosphates, are elevated in fetal brain tissues at E15.5 and E18.5 relative to E10.5. However, almost all nucleotides measured are elevated in E12.5-E18.5 fetal liver tissues relative to E10.5. Specific nucleotides, such as IMP, ADP and ATP, but not AMP, CMP, GMP or UMP, were most elevated in fetal heart tissues at E15.5 and E18.5 relative to E10.5. We were interested to find how purine and pyrimidine metabolism changed across fetal tissue throughout mid-to-late gestation. In placenta and fetal heart, AMP and UMP pool levels did not increase at the developmental stages we measured (Figure 5B and 5C). However, in fetal liver and brain, AMP and UMP pool levels increased (Figure 5B and 5C). Additionally,$^{13}$C enrichment into AMP and UMP consistently decreased across fetal tissues as embryonic day advanced, regardless of pool level changes (Figure 5D and 5E). Similarly, decreasing labeling was observed for IMP and GMP irrespective of pool level trends (Figure S5B–G).

Despite the uniform $^{13}$C-glucose infusion procedure, $^{13}$C enrichment in nucleotides decreased from mid-to late-gestation (Figure 5A and S5A). Nucleotide labeling, which did not reach isotopic steady state in three hours, indicated nucleotide turnover rates. Thus, the decreased labeling that coincided with level or decreased pool sizes implied slower nucleotide biosynthesis fluxes originating from the infused glucose source. We observed that nucleotide biosynthesis from the infused glucose source in the placenta and the heart started slowing down in earlier developmental stages (i.e., E10.5 or E12.5) than in the liver and the brain (i.e., E15.5 or later).

## Histidine-derived metabolites accumulate in late-term fetuses

We expanded our analysis platform to survey all detected LC-MS peaks in an untargeted manner and identify metabolic signatures that characterize developmental transitions. We compared untargeted data from E18.5 and E10.5 placentas harvested from both wildtype and Akita dams (Table S4) using the MetaboAnalyst platform. [22] This analysis yielded histidine metabolism as the metabolic pathway with the highest normalized enrichment score and significance in E18.5 versus E10.5 placentas harvested from wildtype dams (Figure 6A). Similar results were found when comparing placental metabolites from fetuses harvested from Akita dams (Figure S6A). Given the significant enrichment of histidine metabolism in

late stage versus E10.5 placentas, we decided to look more closely at this pathway across fetal tissues and throughout mid-to-late gestation. Histamine is derived from histidine, which can be catabolized to urocanate as well as to histamine (Figure 6B). We found that histidine pool levels did not follow a generalized trend across fetal tissues, and in fact, decreased in fetal hearts and brains isolated from wildtype dams (Figure 6C). However, we observed an accumulation of histidine-derived metabolites at the E18.5 stage in fetal placenta, heart, liver, and brain tissues (Figure 6D–F). In particular, we observed a stark accumulation of the histidine-derived metabolites, histamine, and imidazole-4-acetate (Figure 6E and 6F). These identified signals through untargeted analysis were corroborated by chemical standards (Figure S6B). The increase in histidine-derived metabolites at E18.5 was also observed in maternal circulation (Figure S6C), underscoring the interaction between maternal and fetal metabolism. To examine whether overnight fasting of the dams contributed to the changes observed in histidine catabolism metabolites, we performed LCMS-based metabolomic measurements on E12.5 and E18.5 fetal tissues dissected from both wildtype and Akita dams without fasting and without anesthesia or tracer infusion. In this unperturbed state, we again observed a large increase in histidine-derived metabolites, especially histamine and imidazole-4-acetate, in late-stage fetal tissues regardless of glycemic state, suggesting that the striking increase in histidine metabolism in late-stage fetal tissues is not an effect of overnight fasting of the dams (Figure S6D). Intriguingly, elevated histamine plasma levels have been detected in women during preterm labor compared with term labor. [23]

## DISCUSSION

Our extensive metabolomic dataset presents the first in-depth assessment of *in vivo* fetal tissue metabolism during mid-to-late gestation within the context of both maternal euglycemia and hyperglycemia. Examination of relative metabolite pool levels in fetal tissues revealed elevated levels of the glucose-derived toxic metabolite sorbitol in all fetal tissues examined from hyperglycemic dams (Figure 2). These findings suggest that fetal tissues are not shielded from sorbitol accumulation when developing under maternal hyperglycemia. Uncontrolled high blood glucose in diabetic patients is recognized to lead to sorbitol accumulation and tissue damage in insulin-independent tissues such as retina, kidney, and nerves. [14] Early research hinted at sorbitol accumulation in in rat fetal livers and placentas exposed to maternal hyperglycemia as well as neuroectodermal tissues. [24,25] While sorbitol production in the placenta is well documented in normal pregnancies of several animal species and humans, data regarding the temporal change in the abundance or concentration of sorbitol across gestational stages are scarce. [26,27,28] We now provide a more comprehensive look at the temporal change in sorbitol levels, covering multiple developmental stages and fetal tissues. Although the physiological role of the polyol pathway in normal pregnancy is not well understood and remains to be explored, this pathway has been implicated as a contributor to redox imbalance in diabetes. [29] Our *in vivo* metabolomics data confirms that fetuses from diabetic mice exhibit 3- to 5-fold sorbitol accumulation compared to fetuses from wildtype mice. Further studies should interrogate the impact this amount of sorbitol accumulation has on fetal development. Inhibitors of the sorbitol producing enzyme, aldose reductase, have been used in the clinic to treat diabetic neuropathy. [30] Past research using aldose reductase inhibitors on cultured rat conceptuses

resulted in reduction of sorbitol with no effect on prevention of high glucose-induced growth retardation and dysmorphogenesis. [31] However, more research will be needed to test whether aldose reductase inhibitors can be used to reduce fetal sorbitol levels *in vivo* and if this prevents of some of the developmental defects associated with maternal hyperglycemia.

Additionally, our analysis of relative metabolite pool levels in fetal tissues during mid-to-late gestation revealed altered trends in fetal brain amino acid levels (Figure 3). While each analyzed tissue presented unique trends in amino acid levels throughout mid-to-late gestation, we highlighted those of the brain given the important role certain amino acids have as neurotransmitters in shaping brain networks. [32] At this point, we do not know whether the reduced GABA levels in the fetal brains from Akita dams are due to reduced production or enhanced degradation and follow-up studies are needed to address the mechanistic aspects for this observed trend. Furthermore, while there is growing appreciation on the importance of the glutamatergic system in brain development and function [33], there is a dearth of information on how metabolic abnormalities impact such systems. Therefore, our findings that amino acid neurotransmitters such as aspartate, glutamate, and GABA exhibit different levels in fetal brains isolated from hyperglycemic dams suggest follow-up studies examining whether these alterations may contribute to the higher incidence of congenital brain defects occurring in the context of maternal hyperglycemia.

Beyond understanding metabolite pool level dynamics, we leveraged $^{13}$C-labeling information to investigate fetal tissue central carbon pathway usage as well as nutrient sourcing. For instance, we found that differences in fetal and plasma nutrient labeling from the $^{13}$C-glucose infused into the dam can inform whether a particular nutrient is supplied via maternal circulation or whether it is synthesized by the fetus. Through this analysis, we found that fetal tissues exhibit aspartate and glutamate synthesis throughout mid-to-late gestation, however proline biosynthesis becomes more prominent in late liver and brain development. Additionally, our data suggest that fetal liver tissue derives carbon backbones from a different source than circulating glucose, but less so in the case of maternal hyperglycemia, in which fetuses sustained glucose dependence. This raises an important consideration of carbon sourcing in the developing fetus, particularly at E10.5. In euglycemia, fetuses obtain carbon backbones flexibly via glycogen breakdown or from lactate via gluconeogenesis. Complementing our studies presented here with additional labeling experiments that incorporate other labeled nutrients such as $^{13}$C-lactate represents a logical future direction, which will help illuminate the alternative carbon sources that are relied on by E10.5 livers and hearts from euglycemic and hyperglycemic dams. Notwithstanding, this interesting shift in carbon sourcing in fetuses from hyperglycemic dams highlights the metabolic plasticity and adaptations fetal tissues undergo when challenged with a changing nutrient microenvironment.

Untargeted analyses of our large dataset revealed the striking accumulation of histidine-derived metabolites, including histamine and imidazole-4-acetate, in fetal tissues and maternal plasma at E18.5 (Figure 6). Intriguingly, elevated histamine plasma levels have been detected in women during preterm compared with term labor. [23] These metabolites are therefore of special interest given their potential role in promoting labor. The stark

increase of histidine-derived metabolites we observed as fetuses enter the late stage E18.5 underscores how little is known about the potential role metabolism has in modulating developmental transitions.

Overall, the data resource presented here will help initiate new hypotheses for future testing that will lead to more mechanistic insights connecting metabolism to cell fate transitions. For example, future studies should examine whether metabolites we found elevated in the fetal tissues during diabetic pregnancy are responsible for the increased incidence of congenital defects, as well as determine if sharp metabolite fluctuations delineate important developmental transitions. Better understanding of how maternal metabolism impacts fetal metabolism and development will be crucial to design strategies that promote maternal health and address the urgent clinical issue of diabetic pregnancy.

## LIMITATIONS OF THE STUDY

Although mouse development does not entirely mimic human development, we expect our metabolomic dataset to serve as a valuable complement to extensive studies looking at development through a genomics and transcriptomics lens. Due to the nature of our experiments that necessitated careful timing of pregnancies, we decided to streamline our platform to implement tail vein infusions, which constrained our ability to perform longer infusions and therefore limited the number of metabolites that incorporate the $^{13}$C-label from [U-$^{13}$C]glucose. Given the number of mice infused in this study and the number of fetuses collected, we centered our experimental approach around using a single isotopically labeled nutrient, [U-$^{13}$C]glucose, and the collection of four tissues per fetus dissected. Utilization of additional tracers such as $^{13}$C-glutamine and $^{13}$C-lactate in future studies, will provide additional layers with which to assess pathway use. Testing of additional embryonic days beyond the 4 representative stages we assessed in this study would provide a more precise dissection of fetal metabolic networks. Despite sample normalization, we note that E10.5 fetal livers presented significantly lower metabolite pool levels across many metabolites when compared to E12.5 samples. While this difference was not present among many metabolites, we acknowledge it may be unclear whether this trend has biological value or rather reflects a potential underrepresentation of metabolite pool levels. We recognize that use of the Akita mouse model is one of several approaches that are used to model diabetes in the mouse. Akita mice have dysfunctional insulin due to a mutation in the Ins2 gene that is unable to lower blood glucose levels, which resulted in a larger glucose increase under the glucose tracer infusion parameters used in this study. While the Akita mouse does not perfectly represent all the mechanistic features that may characterize human diabetic pregnancies, our goal with this study was to provide a starting point to analyze the impact high glucose *in utero* has on the metabolism of the developing fetus.

## STAR METHODS

### Lead contact

Further information and requests for resources and reagents should be directed to and will be fulfilled by the Lead Contact, Heather R. Christofk (hchristofk@mednet.ucla.edu).

### Materials availability

This study did not generate new unique reagents.

### Data and code availability

The metabolomics datasets reported in this study have been deposited at the National Metabolomics Data Repository (NMDR) and are publicly as of the date of publication. DOI is listed in the key resources table. This paper does not report original code

## EXPERIMENTAL MODEL AND SUBJECT DETAILS

### Mice

Mice were housed in pathogen-free facilities at University of California Los Angeles (UCLA). All animal experiments were approved by the UCLA Animal Research Committee (ARC), and we complied with all relevant ethical regulations while conducting animal experiments.

## METHOD DETAILS

### Animal studies

Healthy wildtype and Akita dams were set up for timed mating. The following morning, females displaying vaginal plugs were identified as pregnant, recorded as embryonic day (E) 0.5 and moved to a new cage until the appropriate embryonic day to be interrogated.

### Pregnant mouse infusions

Labeled glucose solution was prepared at a concentration of 100 mg/mL in filtered 0.9% sodium chloride solution. After overnight fasting (from 18:00 the day before), infusions took place around between 09:00 and 10:00 for all pregnant dams. Mice were anesthetized using isoflurane gas at 5% and placed on a warm pad. Mice were then kept under 2.5% isoflurane for the duration of infusion. For catheter placement, a 28-gauge insulin syringe needle was connected via polyethylene tubing (PE-10) to a syringe (containing glucose solution) placed on an infusion pump (Harvard Apparatus). At the start of the infusion, the 28-gauge needle was inserted into the tail vein. A glucose bolus of 4 μL/gBW was administered. Right after bolus administration, infusion rate was set at a continuous 0.085ul/gBW/min for a total infusion time of 3 hours.

### Serial cesarean sections

Pregnant mice were placed under a maintained plane of isoflurane anesthesia (2.5%). Retro-orbital blood draw for time zero was performed followed by opening a small incision to the lower abdomen of the pregnant mouse to expose a single conceptus for fetal tissue harvesting. Immediately after the first blood draw and fetus collection, a tail vein catheter was placed and bolus was administered followed by continuous infusion as described in the pregnant mouse infusions method. A single conceptus, accessed via the initial small incision, was harvested at multiple time points during infusion of [U-$^{13}$C]glucose. Retro-orbital blood draws (<20 μL) were taken throughout the infusion to monitor tracer

enrichment in maternal blood. Timepoints for harvesting after time zero were: 30 minutes, 1 hour, 2 hours, 3 hours, and 4 hours.

### Fetal tissue extraction

Mice were euthanized and blood was collected via heart puncture. Fetal tissues (placenta, brain, liver, and heart) were dissected in ice-cold sterile PBS. Immediately after dissection, weight was recorded and fetal tissue was placed in a pre-filled bead mill tube containing metal beads and 500 μL of methanol:water (80:20) solution kept cold on dry ice. Fetal tissues were homogenized using a Fisherbrand™ Bead Mill Homogenizer. Samples were spun at 17,000 g (4 °C) for ten minutes to remove precipitated cell material (protein/DNA). Supernatants were collected, transferred to a clean tube, and evaporated using a Nitrogen evaporator (Organomation). Evaporated metabolite extracts were stored at −80 °C. Pellets containing protein/DNA were dried on a heat block (55 °C) and stored at −80 °C

### Maternal plasma extraction and measurements

Collected blood was centrifuged at 5,000xg to collect plasma. Plasma was snap frozen in liquid nitrogen and stored until extraction. Glucometer was used to determine absolute glucose values from maternal plasma. Insulin measurements were performed by ELISA, following manufacturer instructions (CrystalChem). For metabolite extraction 5 μL plasma was mixed with 500 μL methanol:water (80:20) solution (−80 °C). Samples were centrifuged for ten minutes at 17,000 *g* (4 °C) and 450 μL of each sample was evaporated using a Nitrogen evaporator (Organomation). Evaporated metabolite extracts were stored at −80 °C.

### Fetal tissue DNA measurements and weight normalization

Frozen pellets were resuspended in a solution containing 100mM NaCl, 20mM Tris-HCl (pH 7.4), 5mM EDTA, 0.1% SDS, Proteinase K (500 μg/mL). Volume for pellet resuspension varied per size of fetal tissue pellet to ensure all material was dissolved. Resuspension volume was recorded as a dilution factor. DNA concentration was measured using a nanodrop and total DNA concentration was calculated via dilution factor (Thermo Fisher Scientific).

### Metabolite measurement by LC-MS

Dried metabolite extracts were reconstituted in 50% acetonitrile (ACN) 50% dH20 solution. For fetal liver, brain, and placentas, metabolite extract resuspension volume was set to 75 μL per mg weight. For fetal hearts, metabolite extract resuspension volume was set to 90 μL per mg weight. To increase accuracy in metabolite resuspension volumes, total DNA concentration measurements from each fetal tissue group were correlated to directly measured tissue weights higher than 2mg, and a linear regression equation was used to calculate weight values for tissue samples with recorded weights below 2mg. For plasma metabolite extracts, resuspension volume was set to 100 μL. After resuspension, samples were vortexed and spun down for 10 min at 17,000g. 75 μL of the supernatant was then transferred to HPLC glass vials. Samples were run on a Vanquish (Thermo Scientific) UHPLC system with mobile phase A (20mM ammonium carbonate, pH 9.7) and mobile

phase B (100% ACN) at a flow rate of 150 μL/min on a SeQuant ZIC-pHILIC Polymeric column (2.1 × 150 mm 5 μm, EMD Millipore) at 35°C. Injection volume was set to 10 μL. Separation was achieved with a linear gradient from 20% A to 80% A in 20 min followed by a linear gradient from 80% A to 20% A from 20 min to 20.5 min. 20% A was then held from 20.5 min to 28 min. The UHPLC was coupled to a Q-Exactive (Thermo Scientific) mass analyzer running in polarity switching mode with spray-voltage=3.2kV, sheath-gas=40, aux-gas=15, sweep-gas=1, aux-gas-temp=350°C, and capillary-temp=275°C. For both polarities mass scan settings were kept at full-scan-range=(70–1000), ms1-resolution=70,000, max-injection-time=250ms, and AGC-target=1E6. MS2 data was also collected from the top three most abundant singly charged ions in each scan with normalized-collision-energy=35. Each resulting .raw files was centroided and converted into two .mzXML files (one for positive ion mode scans and one for negative ion mode scans) using msconvert from ProteoWizard. [34]

## QUANTIFICAITON AND STATISTICAL ANALYSIS

### Metabolomic data analysis

.mzXML files were imported into the MZmine 2 software package. [35] Ion chromatograms were generated from MS1 spectra via the built-in Automated Data Analysis Pipeline (ADAP). [36] Chromatogram module and peaks were detected via the ADAP wavelets algorithm. Peaks were aligned across all samples via the Random sample consensus aligner module, gap-filled, and assigned identities using an exact mass MS1(±15ppm) and retention time RT (±0.5min) search of our in-house MS1-RT database. Peak boundaries and identifications were then further refined by manual curation. Peaks were quantified by area under the curve integration and exported as .CSV files. For isotopologue analysis, peak areas were processed via the R package AccuCor to correct for natural isotope abundance. [37] Peak selection for untargeted metabolomic analysis was performed using El-Maven (Elucidata) automatic feature detection. Functional analysis annotation of untargeted data was performed using MetaboAnalyst 5.0, using peak intensity tables as input, with a mass tolerance set at 15 ppm, and processing the data through an interquartile range (IQR) filter, a log base 10 transformation, and the automatic data scaling feature. [22] Gene set enrichment analysis algorithm, integrated in the MetaboAnalyst pipeline was applied using the KEGG (*mus musculus*) database as reference.

### Analysis of labeling dynamics

The time development of isotope enrichment in both maternal plasma and fetal tissues was analyzed by graphing the weighted glucose enrichment at each of the timepoints probed during serial cesarean sections (0 min, 30 min, 1h, 2h, and 4h). Two mathematical approaches were applied to assess steady-state at three hours of tracer infusion. The first approach applied for steady-state assessment of glucose in maternal plasma involved calculating the rate of change in the labeled fraction, which is represented by the slope of a linear regression analysis. Using this information, we calculated the nmol change in labeled glucose over time by considering the upper limit of the variable glucose concentration range of 100–500 mg/dL and the variable blood volume of 77–80 mL/kg mouse weight. [38] Using these metrics, the change in labeled glucose was calculated and compared to previously

reported overall circulatory turnover flux of glucose in mice, 150.9 ± 46.7 nmol/g/min [20], which is two orders of magnitude faster than the observed changes in labeled glucose in this study, 1.67 nmol/g/min (Figure S1).

A second approach applied to both maternal plasma glucose and fetal tissue glucose involved fitting an exponential rise to maximum (one-phase association) model.

$$L = P\left(1 - e^{-kt}\right)$$

Where $L$ is the labeled fraction, $P$ is the labeling plateau, t is time in hours, and $k$ is the rate constant in $h^{-1}$. A larger $k$t value (where t is equal to 3 hours for our main results) relative to the plateau $P$ was suggestive of (pseudo-)steady state (Figure S1).

## Interpretation of metabolite isotopologue distributions

Carbon labeling of metabolite pools was analyzed in two ways, either by the fraction of its highest labeled isotopologue (i.e. M+6 for a 6-carbon metabolite) or by the weighted average of all isotopologues to give the total fractional carbon labeling (i.e. the proportion of individual carbon atoms in the metabolite pool that are labeled).

$$Fraction\ of\ carbons\ that\ are\ ^{13}C = \sum_{i=0}^{N} P_i \frac{i}{N}$$

Here, N is the number of carbon atoms in the metabolite and $P_i$ is the fractional abundance of the M+i isotopologue.

To determine the expected fractional abundance of labeling in each pathway (Figure 1E), we used all measured metabolites in respective pathways (denoted in black text in the pathway panel of Figure 1E) and the fractional abundance of all labeled isotopologues. Metabolites colored gray in the pathway panel of Figure 1E were not measured. For each pathway, the reported value represents the mean of the fractions of carbons that are $^{13}C$ in the metabolites.

$$E(\%\ carbons\ labeled\ in\ pathway) = \frac{1}{M} \sum_{m=1}^{M} \sum_{i=1}^{N_m} P_{m,i} \frac{i}{N_m}$$

Here, $m$ is each metabolite in a pathway with total number of metabolites M, $i$ is each isotopologue of a metabolite with a total of $N_m$ carbons, and $P_{m,i}$ is the fractional abundance of isotopologue $i$ in metabolite $m$.

## Statistical Analysis

To highlight the number of substantial differences in our targeted metabolomics datasets two-way ANOVA with a Benjamini-Hochberg FDR controlling procedure was used,

pinpointing significant metabolite changes across both factors (glycemic state and embryonic day) as well as via potential interaction effects, following log transformation and imputation of missing values. When representing relative metabolite abundances, statistical significance was determined via multiple two-tailed *t*-tests with adjustment using the Benjamini-Hochberg FDR controlling method to correct for multiple testing across all relevant comparisons presented in this study (glycemic state comparisons for each developmental stage, and developmental stage comparisons for each glycemic state). For labeling data, statistical significance was determined via multiple two-tailed *t*-tests with Holm-Sidak's multiple-comparisons adjustment. Data presented as box plots had Tukey method applied to define whiskers and outliers. Data presented as individual values include mean ± s.e.m. Significance representation was n.s., not significant, $^{*}p < 0.05$, $^{**}p < 0.01$, $^{***}p < 0.001$, and $^{****}p < 0.0001$. Sample number for metabolomics analysis was as follows: placenta, n=121; fetal heart, n=120; fetal liver n=121; fetal brain=120; maternal plasma, n=32.

## Supplementary Material

Refer to Web version on PubMed Central for supplementary material.

## ACKNOWLEDGMENTS

We thank the UCLA Crump Preclinical Imaging Technology Center for providing equipment for mouse *in vivo* tracing, and all members of the Christofk laboratory for discussion and constructive feedback. CAP was supported by UCLA's Broad Stem Cell Research Center (BSCRC) Training Program. Research funding for this study was provided by UCLA's BSCRC Innovation Award given to HRC, AN, and JOP. JOP was funded by R35 GM143127. AN was funded by R01 HL142801. HRC was funded by R01 CA215185, R01 AR070245.

## REFERENCES

1. Georgieff MK (2020). Iron deficiency in pregnancy. Am. J. Obstet. Gynecol 223, 516–524. [PubMed: 32184147]
2. Scholl TO, and Johnson WG (2000). Folic acid: influence on the outcome of pregnancy. Am. J. Clin. Nutr 71, 1295S–1303S. [PubMed: 10799405]
3. Sharpley MS, Chi F, Ten Hoeve J, and Banerjee U (2021). Metabolic plasticity drives development during mammalian embryogenesis. Dev. Cell 56, 2329–2347. e2326. [PubMed: 34428399]
4. Solmonson A, Faubert B, Gu W, Rao A, Cowdin MA, Menendez-Montes I, Kelekar S, Rogers TJ, Pan C, and Guevara G (2022). Compartmentalized metabolism supports midgestation mammalian development. Nature 604, 349–353. [PubMed: 35388219]
5. Shah NS, Wang MC, Freaney PM, Perak AM, Carnethon MR, Kandula NR, Gunderson EP, Bullard KM, Grobman WA, O'Brien MJ, and Khan SS (2021). Trends in Gestational Diabetes at First Live Birth by Race and Ethnicity in the US, 2011–2019. JAMA 326, 660–669. 10.1001/jama.2021.7217. [PubMed: 34402831]
6. Øyen N, Diaz LJ, Leirgul E, Boyd HA, Priest J, Mathiesen ER, Quertermous T, Wohlfahrt J, and Melbye M (2016). Prepregnancy diabetes and offspring risk of congenital heart disease: a nationwide cohort study. Circulation 133, 2243–2253. [PubMed: 27166384]
7. Tinker SC, Gilboa SM, Moore CA, Waller DK, Simeone RM, Kim SY, Jamieson DJ, Botto LD, Reefhuis J, and Study NBDP (2020). Specific birth defects in pregnancies of women with diabetes: National Birth Defects Prevention Study, 1997–2011. Am. J. Obstet. Gynecol 222, 176. e171–176. e111.
8. Ornoy A, Becker M, Weinstein-Fudim L, and Ergaz Z (2021). Diabetes during pregnancy: A maternal disease complicating the course of pregnancy with long-term deleterious effects on the offspring. a clinical review. Int. J. Mol. Sci 22, 2965. [PubMed: 33803995]

9. Nakano H, Minami I, Braas D, Pappoe H, Wu X, Sagadevan A, Vergnes L, Fu K, Morselli M, and Dunham C (2017). Glucose inhibits cardiac muscle maturation through nucleotide biosynthesis. Elife 6, e29330. [PubMed: 29231167]
10. Chen A, Liao S, Cheng M, Ma K, Wu L, Lai Y, Qiu X, Yang J, Xu J, and Hao S (2022). Spatiotemporal transcriptomic atlas of mouse organogenesis using DNA nanoball-patterned arrays. Cell 185, 1777–1792. e1721. [PubMed: 35512705]
11. He P, Williams BA, Trout D, Marinov GK, Amrhein H, Berghella L, Goh S-T, Plajzer-Frick I, Afzal V, and Pennacchio LA (2020). The changing mouse embryo transcriptome at whole tissue and single-cell resolution. Nature 583, 760–767. [PubMed: 32728245]
12. Gorkin DU, Barozzi I, Zhao Y, Zhang Y, Huang H, Lee AY, Li B, Chiou J, Wildberg A, and Ding B (2020). An atlas of dynamic chromatin landscapes in mouse fetal development. Nature 583, 744–751. [PubMed: 32728240]
13. Yoshioka M, Kayo T, Ikeda T, and Koizuni A (1997). A novel locus, Mody4, distal to D7Mit189 on chromosome 7 determines early-onset NIDDM in nonobese C57BL/6 (Akita) mutant mice. Diabetes 46, 887–894. [PubMed: 9133560]
14. Brownlee M (2001). Biochemistry and molecular cell biology of diabetic complications. Nature 414, 813–820. [PubMed: 11742414]
15. Represa A, and Ben-Ari Y (2005). Trophic actions of GABA on neuronal development. Trends Neurosci 28, 278–283. [PubMed: 15927682]
16. Linask KK, Han M, and Bravo-Valenzuela NJ (2014). Changes in vitelline and utero-placental hemodynamics: implications for cardiovascular development. Front. Physiol 5, 390. [PubMed: 25426076]
17. Kiserud T (2005). Physiology of the fetal circulation. Semin. Fetal Neonatal Med 10, 493–503. [PubMed: 16236564]
18. Baumann MU, Deborde S, and Illsley NP (2002). Placental glucose transfer and fetal growth. Endocrine 19, 13–22. [PubMed: 12583599]
19. Lager S, and Powell TL (2012). Regulation of nutrient transport across the placenta. J. Pregnancy 2012.
20. Hui S, Ghergurovich JM, Morscher RJ, Jang C, Teng X, Lu W, Esparza LA, Reya T, Zhan L, and Yanxiang Guo J (2017). Glucose feeds the TCA cycle via circulating lactate. Nature 551, 115–118. [PubMed: 29045397]
21. TeSlaa T, Bartman CR, Jankowski CS, Zhang Z, Xu X, Xing X, Wang L, Lu W, Hui S, and Rabinowitz JD (2021). The source of glycolytic intermediates in mammalian tissues. Cell Metab 33, 367–378. e365. [PubMed: 33472024]
22. Pang Z, Zhou G, Ewald J, Chang L, Hacariz O, Basu N, and Xia J (2022). Using MetaboAnalyst 5.0 for LC–HRMS spectra processing, multi-omics integration and covariate adjustment of global metabolomics data. Nat. Protoc, 1–27. [PubMed: 34873329]
23. Maintz L, Schwarzer V, Bieber T, van der Ven K, and Novak N (2008). Effects of histamine and diamine oxidase activities on pregnancy: a critical review. Hum. Reprod. Update 14, 485–495. [PubMed: 18499706]
24. Eriksson U, Naeser P, and Brolin S (1986). Increased accumulation of sorbitol in offspring of manifest diabetic rats. Diabetes 35, 1356–1363. [PubMed: 3770312]
25. Sussman I, and Matschinsky FM (1988). Diabetes affects sorbitol and myo-inositol levels of neuroectodermal tissue during embryogenesis in rat. Diabetes 37, 974–981. [PubMed: 3384192]
26. Teng CC, Tjoa S, Fennessey PV, Wilkening RB, and Battaglia FC (2002). Transplacental carbohydrate and sugar alcohol concentrations and their uptakes in ovine pregnancy. Exp. Biol. Med. (Maywood) 227, 189–195. [PubMed: 11856817]
27. Jauniaux E, Hempstock J, Teng C, Battaglia FC, and Burton GJ (2005). Polyol concentrations in the fluid compartments of the human conceptus during the first trimester of pregnancy: maintenance of redox potential in a low oxygen environment. J. Clin. Endocrinol. Metab 90, 1171–1175. [PubMed: 15562012]
28. Brusati V, Jóźwik M, Jóźwik M, Teng C, Paolini C, Marconi AM, and Battaglia FC (2005). Fetal and maternal non-glucose carbohydrates and polyols concentrations in normal human pregnancies at term. Pediatr. Res 58, 700–704. [PubMed: 16189196]

29. Yan L.j. (2018). Redox imbalance stress in diabetes mellitus: Role of the polyol pathway. Animal models and experimental medicine 1, 7–13. [PubMed: 29863179]

30. Schemmel KE, Padiyara RS, and D'Souza JJ (2010). Aldose reductase inhibitors in the treatment of diabetic peripheral neuropathy: a review. J. Diabetes Complications 24, 354–360. [PubMed: 19748287]

31. Hod M, Star S, Passonneau JV, Unterman TG, and Freinkel N (1986). Effect of hyperglycemia on sorbitol and myo-inositol content of cultured rat conceptus: failure of aldose reductase inhibitors to modify myo-inositol depletion and dysmorphogenesis. Biochem. Biophys. Res. Commun 140, 974–980. [PubMed: 3096334]

32. Kölker S (2018). Metabolism of amino acid neurotransmitters: the synaptic disorder underlying inherited metabolic diseases. J. Inherit. Metab. Dis 41, 1055–1063. [PubMed: 29869166]

33. Matsugami TR, Tanemura K, Mieda M, Nakatomi R, Yamada K, Kondo T, Ogawa M, Obata K, Watanabe M, and Hashikawa T (2006). Indispensability of the glutamate transporters GLAST and GLT1 to brain development. Proc. Natl. Acad. Sci. USA 103, 12161–12166. [PubMed: 16880397]

34. Chambers MC, Maclean B, Burke R, Amodei D, Ruderman DL, Neumann S, Gatto L, Fischer B, Pratt B, and Egertson J (2012). A cross-platform toolkit for mass spectrometry and proteomics. Nat. Biotechnol 30, 918–920. [PubMed: 23051804]

35. Pluskal T, Castillo S, Villar-Briones A, and Orešič M (2010). MZmine 2: modular framework for processing, visualizing, and analyzing mass spectrometry-based molecular profile data. BMC Bioinformatics 11, 1–11. [PubMed: 20043860]

36. Myers OD, Sumner SJ, Li S, Barnes S, and Du X (2017). One step forward for reducing false positive and false negative compound identifications from mass spectrometry metabolomics data: new algorithms for constructing extracted ion chromatograms and detecting chromatographic peaks. Anal. Chem 89, 8696–8703. [PubMed: 28752754]

37. Su X, Lu W, and Rabinowitz JD (2017). Metabolite spectral accuracy on orbitraps. Anal. Chem 89, 5940–5948. [PubMed: 28471646]

38. Mitruka BM, and Rawnsley HM (1981). Clinical biochemical and hematological reference values in normal experimental animals (Masson Publishing USA Inc.).

**HIGHLIGHTS:**

- Metabolomic profiling reveals maternal hyperglycemia impacts fetal metabolism
- Sorbitol accumulates in fetal tissues from hyperglycemic dams
- $^{13}$C-glucose tracing shows maternal hyperglycemia alters fetal nutrient sourcing
- Histidine-derived metabolites accumulate in late-stage fetal tissues

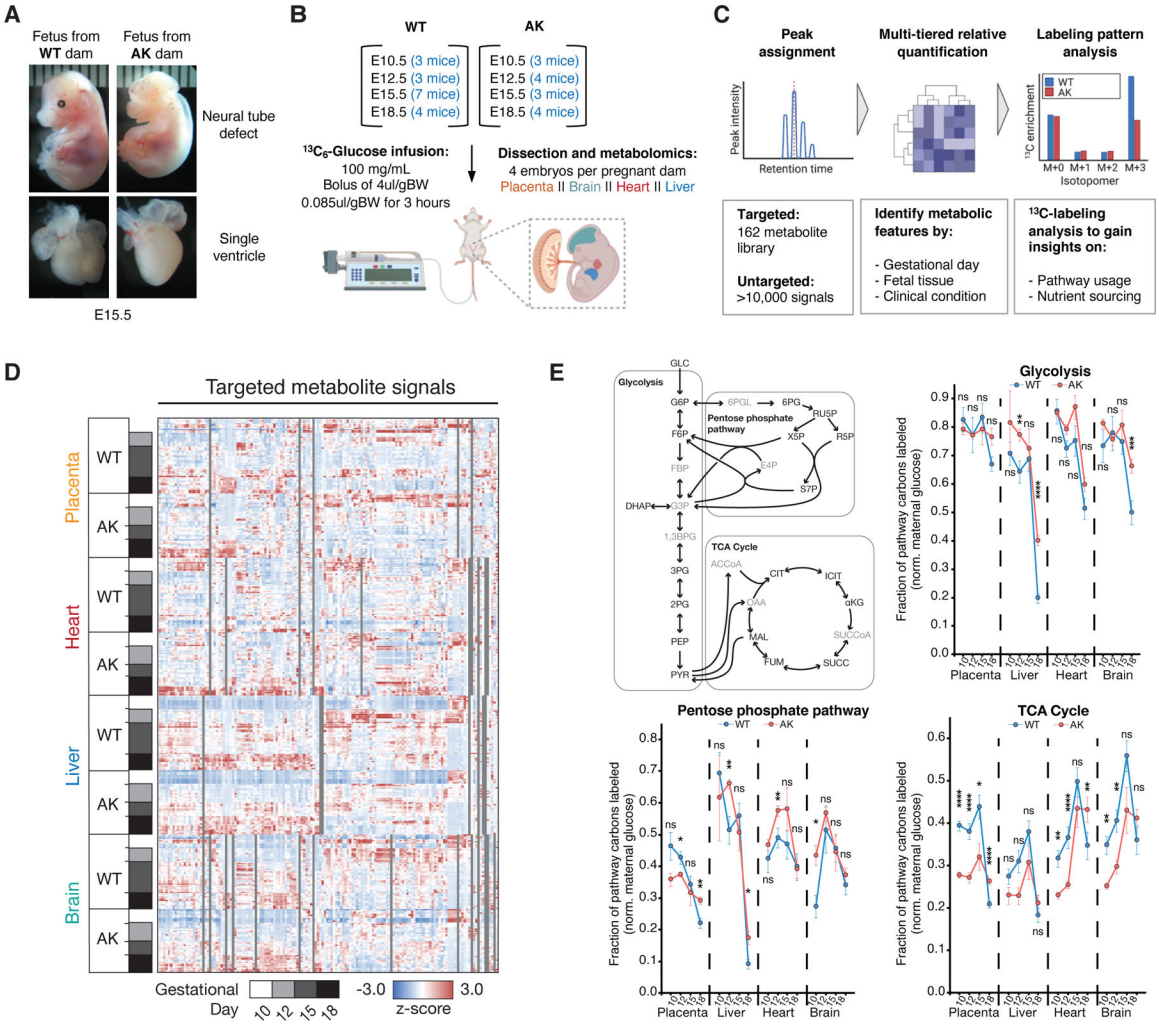


**Figure 1. Metabolomic platform to assess fetal metabolism during mid-to-late gestation and diabetic pregnancy.**

(A) Images of fetuses harvested from wildtype (WT) and Akita (AK) dams at embryonic day 15.5 highlighting neural tube defect and single ventricle defect in fetuses from Akita dams. (B) Schematic of experimental setup involving timed pregnancies in WT and AK dams, [U-$^{13}C_6$]glucose infusion parameters, and tissues collected. (C) Schematic of LC-MS-based metabolomic data analysis approach. (D) Heatmap representation of targeted metabolite analysis across placenta, heart, liver, and brain in fetal tissues isolated from WT and AK dams across multiple timepoints during development. The plotted data represents z-score. Gray indicates not detected across fetal tissue set. (E) The expected fraction of pathway carbons labeled normalized to the level of maternal glucose labeling. Fractional labeling of carbons from metabolites in a pathway (glycolysis, pentose phosphate pathway, TCA cycle) was averaged and weighted by the number of carbons per metabolite to indicate whole pathway labeling at different timepoints during mid-to-late gestation. Metabolites colored gray in the pathway panel were not measured. Statistical analyses were performed using multiple two-tailed *t*-tests with Holm-Sidak's multiple-comparisons adjustment.

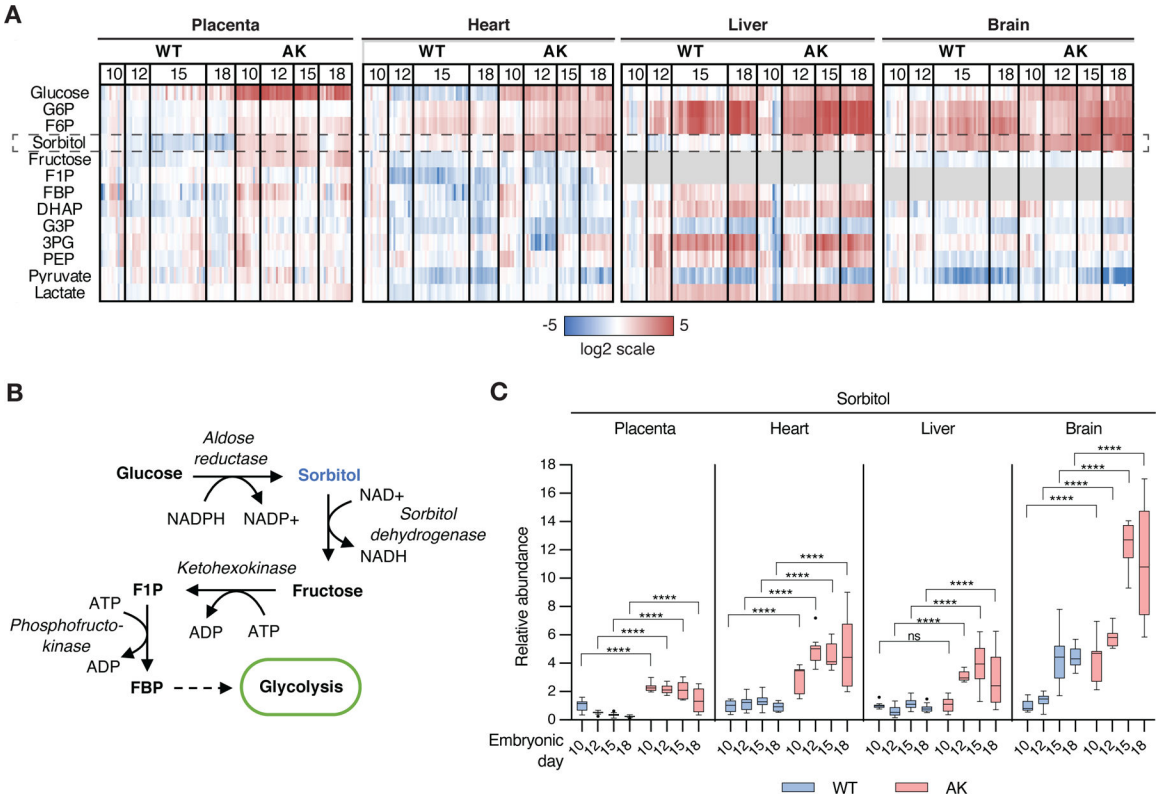


**Figure 2. Maternal hyperglycemia causes sorbitol accumulation in fetal tissues.**

(A) Heatmap representing the log2 fold changes in glycolytic and polyol pathway intermediates relative to E10.5 fetal tissues from wildtype (WT) dams. Gray indicates not detected. (B) Schematic of the polyol pathway and its intersection with glycolysis. (C) Sorbitol pool levels in fetal tissues isolated from WT and AK dams. Data represented as a relative comparison to E10.5 fetal tissues from WT dams. Individual values are plotted relative to the mean of WT E10.5. Tukey method was applied for plotting whiskers and outliers. Statistical analyses were performed via multiple two-tailed *t*-tests with adjustment using the Benjamini-Hochberg FDR controlling method. G6P, glucose-6-phosphate; F6P, fructose-6-phosphate, F1P, fructose-1-phosphate; FBP, fructose bisphosphate; DHAP, dihydroxyacetone phosphate; G3P, glyceraldehyde-3-phosphate; 3PG, 3-phosphoglycerate; PEP, phosphoenolpyruvate.

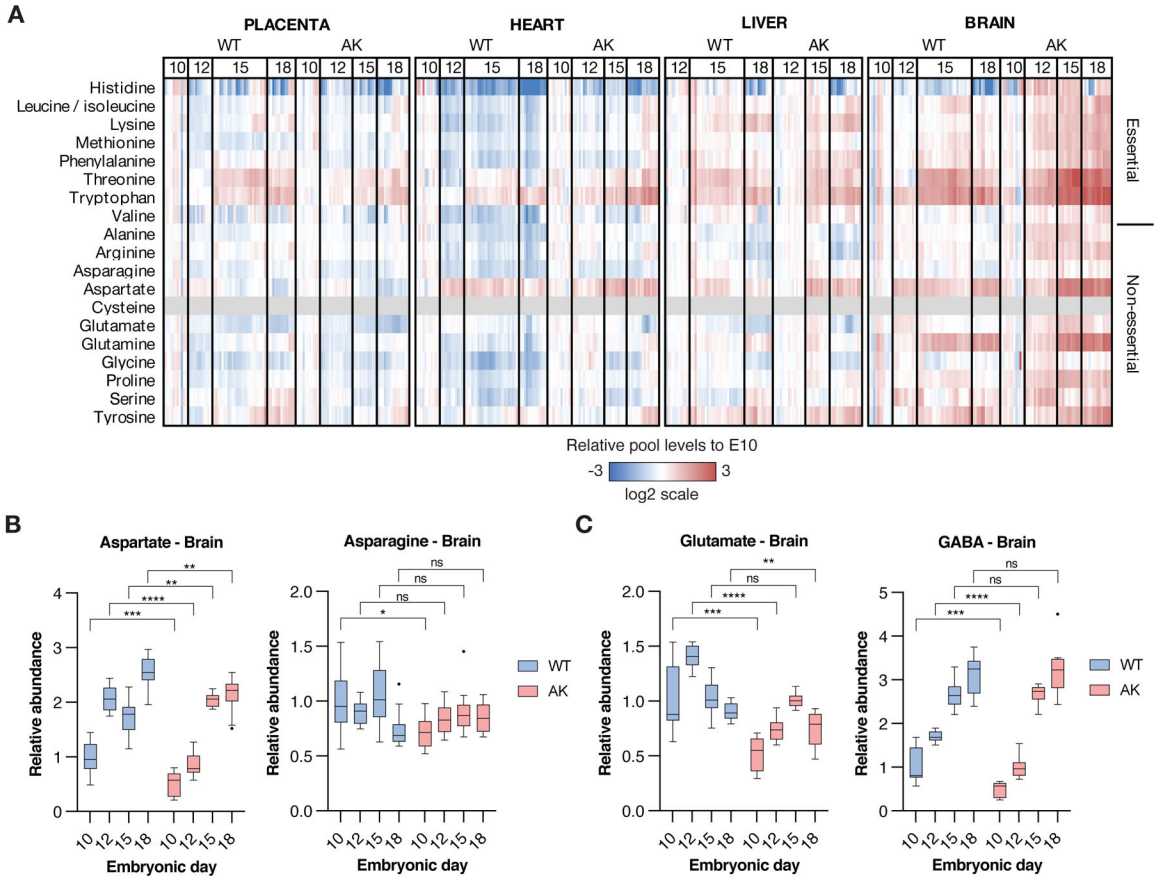


**Figure 3. Maternal hyperglycemia alters aspartate and glutamate levels in fetal brains during mid-to-late gestation.**

(A) Heatmap representing the log2 fold changes in amino acid pool levels relative to E10.5 fetal tissues isolated from both wildtype (WT) and Akita (AK) dams. For fetal tissues from WT dams, data is represented relative to the WT E10.5 samples. For fetal tissues from AK dams, data is represented relative to the average of AK E10.5 samples (B) Relative aspartate and asparagine levels in fetal brain tissues. Data represented relative to E10.5 fetal brain tissues from WT dams. Tukey method was applied for plotting whiskers and outliers. Statistical analyses were performed via multiple two-tailed *t*-tests with adjustment using the Benjamini-Hochberg FDR controlling method. (C) Relative glutamate and GABA levels in fetal brain tissues. Data represented relative to E10.5 fetal brain tissues from WT dams. Tukey method was applied for plotting whiskers and outliers. Statistical analyses were performed via multiple two-tailed *t*-tests with adjustment using the Benjamini-Hochberg FDR controlling method.

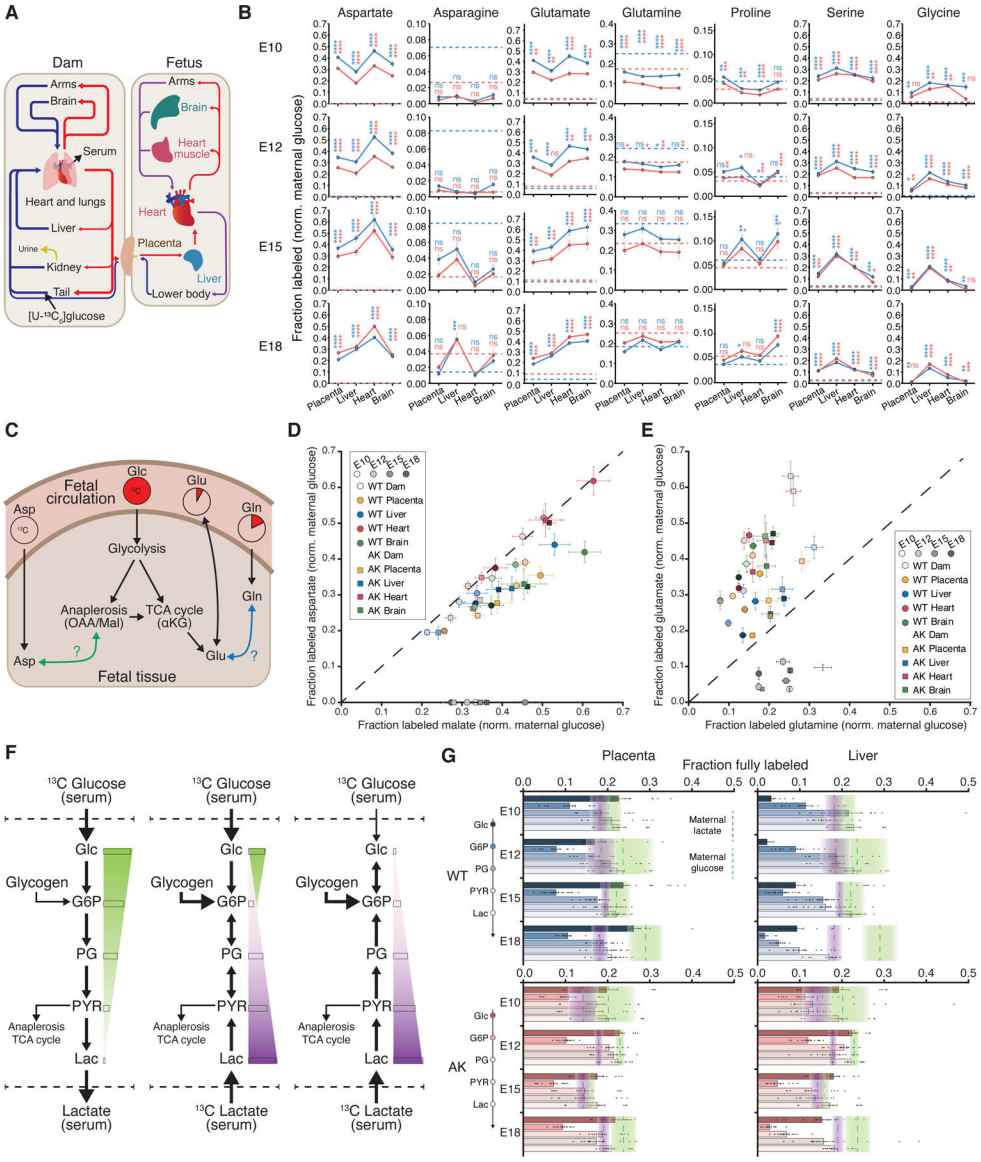


**Figure 4. Isotope tracing in fetal tissues elucidates fetal nutrient sourcing and utilization.**

(A) Schematic of fetal circulation from the dam to the fetus. Nutrients from the dam are transferred through the placenta and into fetal circulation, where the liver, heart, and brain can uptake nutrients supplied via the dam. (B) Tracing of seven amino acids, which were labeled in fetal tissues, through fetal circulation. Labeling across four fetal tissues (placenta, liver, heart, brain) was compared to the labeling of circulating amino acids in the maternal bloodstream (dashed line). Blue lines indicate amino acid labeling in fetal tissues from WT dams, and red lines indicate labeling in fetal tissues from Akita dams. Statistics between the tissue and dam were performed under a two-tailed *t*-test. (C) Schematic of the sources of non-essential amino acids. (D) Labeling of aspartate and malate across fetal tissue and maternal plasma. The dashed line represents the line of unity, where malate and aspartate labeling are equal. (E) Labeling of glutamate and glutamine across fetal tissue and maternal plasma. (F) Depiction of three major carbon sources for glycolytic intermediates

and biomass building blocks. Glycolysis and gluconeogenesis both can supply $^{13}C$ to glycolytic intermediates. The labeling of glycolytic intermediates may follow labeling of either glucose (green) or lactate (purple). Glycogen, which is unlabeled, may dilute labeling of glycolytic intermediates. (G) Fraction of fully labeled glycolytic intermediates (glucose, glucose-6-phosphate, phosphoglycerate, pyruvate, lactate) in WT and AK placenta and liver compared to maternal glucose and lactate labeling. Green bands represent maternal plasma labeling of glucose, and purple bands represent maternal labeling of lactate. Mean ± s.e.m. are represented by a dashed line and the width of the bands.

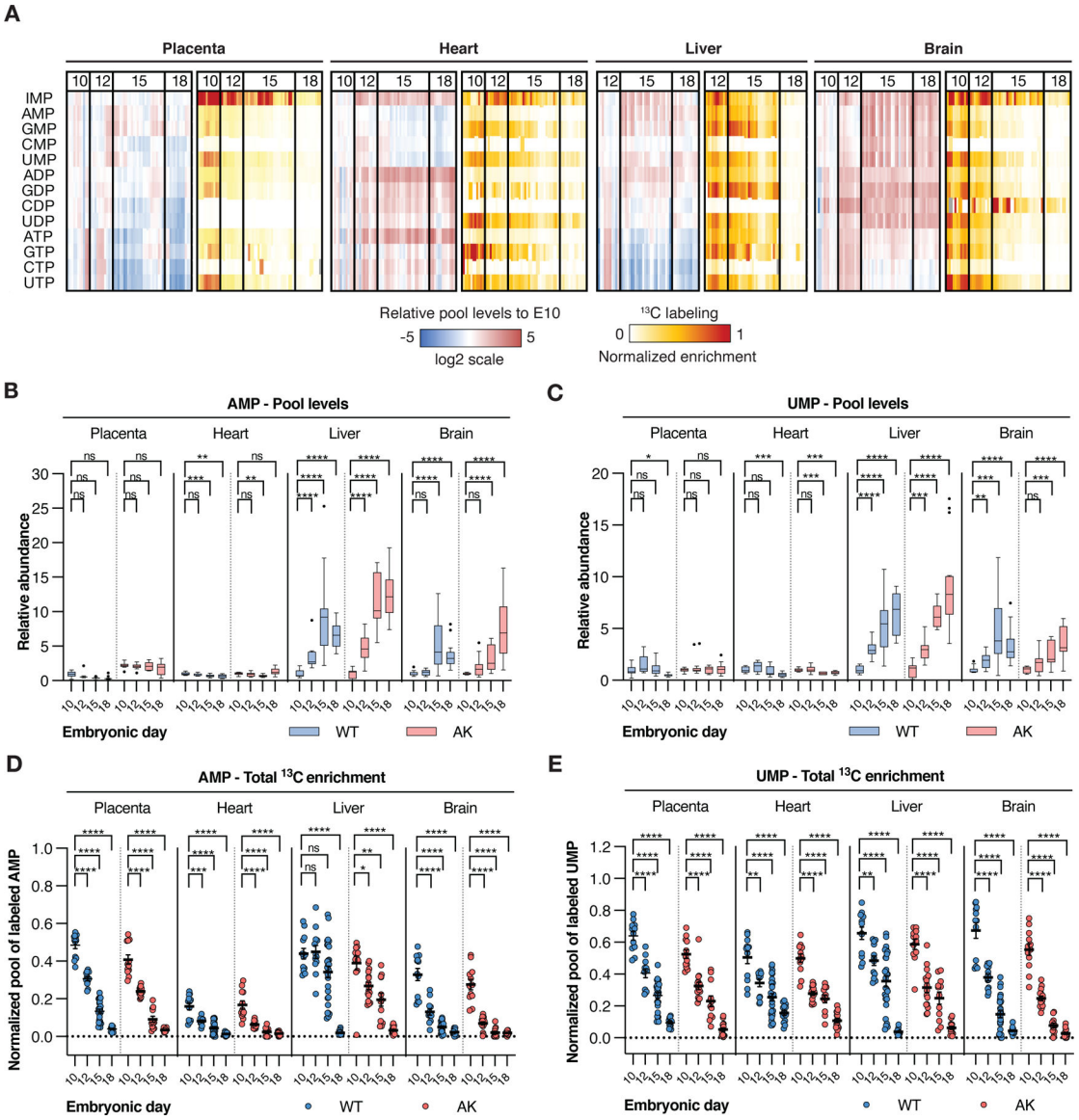


**Figure 5. Progressive decrease in *de novo* nucleotide synthesis during fetal development.**

(A) Blue to red scale: Heatmap representing the log2 fold changes in nucleotide pool levels relative to E10.5 fetal tissues (placenta, heart, and brain) or E12.5 for fetal livers from WT dams. White to red scale: Heatmap representing the total $^{13}$C-enrichment (1-unlabeled) of nucleotides in fetal tissues from WT dams. (B-C) Relative AMP (B) and UMP (C) pool levels across fetal tissues. For fetal tissues from WT dams, data is represented relative to the mean of WT E10.5 samples. For fetal tissues from Akita (AK) dams, data is represented relative to the mean of AK E10.5 samples. Tukey method was applied for plotting whiskers and outliers. Statistical analyses were performed via multiple two-tailed *t*-tests with adjustment using the Benjamini-Hochberg FDR controlling method. (D-E) Normalized total $^{13}$C-enrichment (1-unlabeled) of AMP (D) and UMP (E) across fetal tissues. For each fetal tissue sample, the nucleotide labeled pool (1-unlabeled) was normalized to its respective total $^{13}$C-enrichment (1-unlabeled) of glucose from maternal plasma. Data are individual

points and mean ± s.e.m. Statistical analyses were performed using multiple two-tailed *t*-tests with Holm-Sidak's multiple-comparisons adjustment.

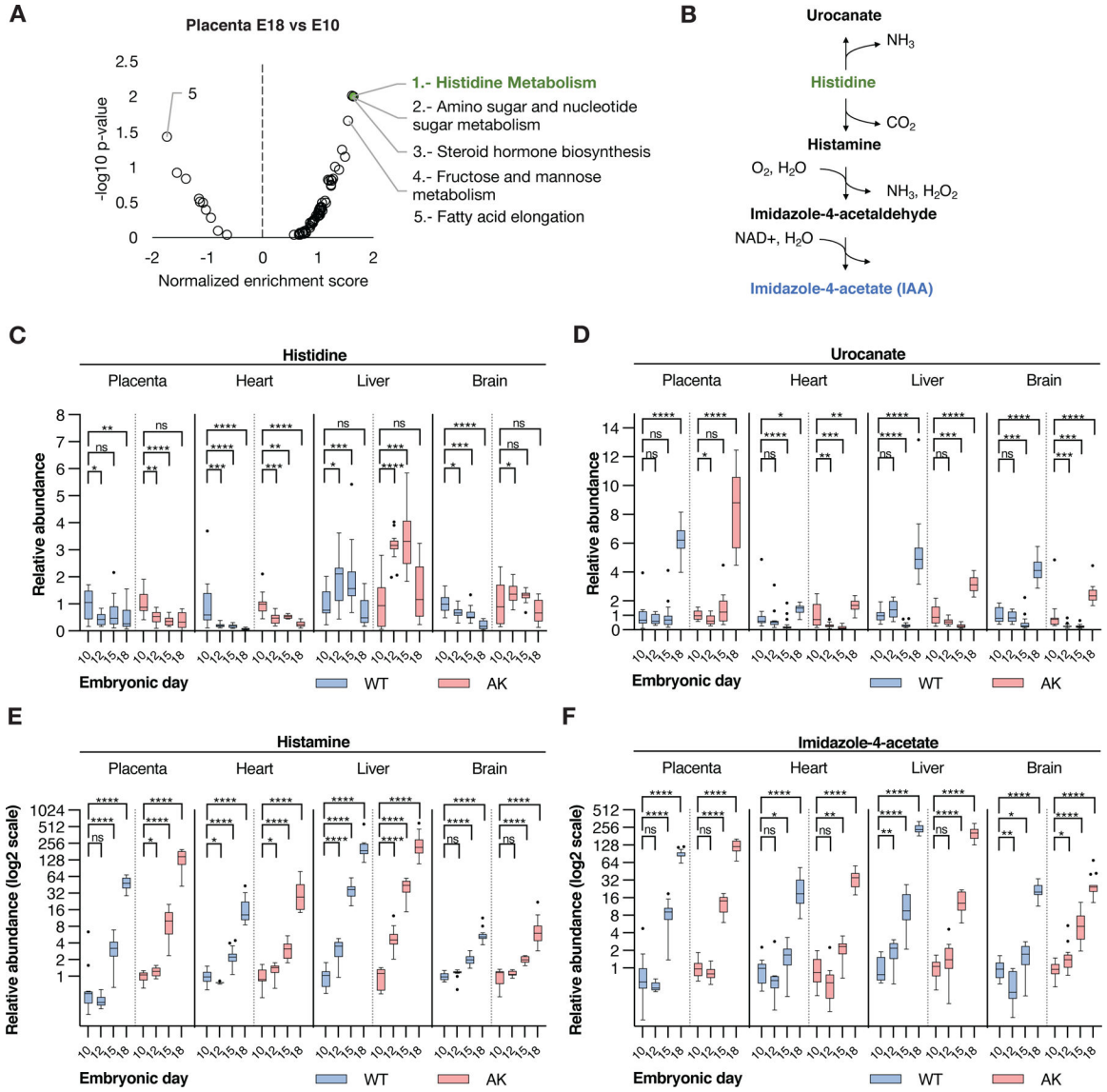


**Figure 6. Histidine-derived metabolites accumulate in fetal tissues during late development.**

(A) MetaboAnalyst pathway analysis using positive ion mode untargeted data highlights changes in histidine metabolism in placenta E18.5 tissues relative to E10.5 from wildtype dams with representation of raw p-values. Top 5 pathway terms are listed (B) Histidine metabolism pathway schematic. (C-F): Relative pool levels of histidine (C) and its derived metabolites, urocanate (D), histamine (E), and imidazole-4-acetate (F) across fetal tissues from both wildtype (WT) and Akita (AK) dams. For fetal tissues from WT dams, data is represented relative to the mean of WT E10.5 samples. For fetal tissues from Akita (AK) dams, data is represented relative to the mean of AK E10.5 samples. Relative pool levels of histamine (E) and imidazole-4-acetate (F) are shown using a log2 scale for the y-axis. Tukey method was applied for plotting whiskers and outliers. Statistical analyses were performed using multiple two-tailed *t*-tests with adjustment using the Benjamini-Hochberg FDR controlling method.

## Key resources table

| REAGENT or RESOURCE | SOURCE | IDENTIFIER |
|---|---|---|
| Antibodies | | |
| Bacterial and virus strains | | |
| Biological samples | | |
| Chemicals, peptides, and recombinant proteins | | |
| Methanol; LC-MS grade | Fisher Scientific | Cat#: A456-212 |
| Acetonitrile; LC-MS grade | Fisher Scientific | Cat#: A955-4 |
| Water, LC-MS grade | Fisher Scientific | Cat#: W6-4 |
| Ammonium carbonate | Sigma Aldrich | Cat#: 379999-50G |
| [U-13C]glucose | Cambridge Isotopes | Cat#: CLM-1396 |
| Critical commercial assays | | |
| Insulin ELISA kit | Crystal Chem | Cat#: 50-194-7920 |
| Deposited data | | |
| Fetal tissue and maternal plasma metabolomics | http://dx.doi.org/10.21228/M83139 | NMDR: PR001761 |
| Experimental models: Cell lines | | |
| Experimental models: Organisms/strains | | |
| Mouse strain: C57BL/6J | The Jackson Laboratories | Cat#: 000664 |
| Mouse strain: C57BL/6-*Ins2*$^{Akita}$/J | The Jackson Laboratories | Cat#: 003548 |
| Oligonucleotides | | |
| Recombinant DNA | | |
| Software and algorithms | | |
| Prism 10 | Graphpad | https://www.graphpad.com/scientificsoftware/prism/ |
| MZmine 2 | Github | http://mzmine.github.io/ |
| Accucor | Github | https://github.com/lparsons/accucor |
| El-MAVEN | Elucidata | https://resources.elucidata.io/elmaven/ |
| MetaboAnalyst | Pang et al.[22] | https://www.metaboanalyst.ca/ |
| Other | | |
| Q Exactive | Thermo Fisher | N/A |
| BeadMill Homogenizer | Fisher Scientific | Cat#: 15-340-163 |
| Vanquish UHPLC | Thermo Fisher | N/A |
| SeQuant ZIC-pHILIC Polymeric column (2.1 × 150 mm 5 μm) | EMD Millipore | Cat#: 150460 |
| 2mL tubes pre-filled with 2.4mm metal beads | Fisher Scientific | Cat#: 15-340-151 |
| Infusion pump | Harvard Apparatus | Cat#: HA1100 |
| Nitrogen evaporator | Organomation | Cat#: 11250-O |
| Polyethylene tubing | Instech | Cat#: BTPE-10 |